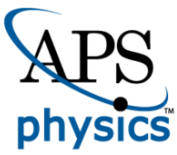

Superconductivity in the Surface State of Noble Metal Gold and its Fermi Level Tuning by EuS Dielectric

Peng Wei, Sujit Manna, Marius Eich, Patrick Lee, and Jagadeesh Moodera

Phys. Rev. Lett. **122**, 247002 — Published 21 June 2019

DOI: 10.1103/PhysRevLett.122.247002

Superconductivity in the surface state of noble metal gold and its Fermi level tuning by EuS dielectric

Authors: Peng Wei[1,3†*], Sujit Manna[1†*], Marius Eich[2,4], Patrick Lee[1*] and Jagadeesh Moodera[1,2*]

Affiliations:

1. Department of Physics, Massachusetts Institute of Technology, Cambridge, MA 02139, United States
2. Plasma Science and Fusion Center & Francis Bitter Magnet Laboratory, Massachusetts Institute of Technology, Cambridge, MA 02139, United States
3. Department of Physics and Astronomy, University of California, Riverside, CA 92521, United States
4. Solid State Physics Laboratory, ETH Zurich, 8093 Zurich, Switzerland

† These authors contributed equally to this work

* Correspondence should be addressed to:

peng.wei@ucr.edu

smanna@mit.edu

palee@mit.edu

moodera@mit.edu

Abstract:

The induced superconductivity (SC) in a robust and scalable quantum material with strong Rashba spin-orbit coupling is particularly attractive for generating topological superconductivity and Majorana bound states (MBS). Gold (111) thin film has been proposed as a promising candidate because of the large Rashba energy, the predicted topological nature and the possibility for large-scale MBS device fabrications.[1] We experimentally demonstrate two important steps towards achieving such a goal. We successfully show induced SC in the Shockley surface state (SS) of ultrathin Au(111) layers grown over epitaxial vanadium films, which is easily achievable on a wafer scale. The emergence of SC in the SS, which is physically separated from a bulk superconductor, is attained by indirect quasiparticle scattering processes instead of by conventional interfacial Andreev reflections.[1] We further show the ability to tune the SS Fermi level (E_F) by interfacing SS with a high-κ dielectric ferromagnetic insulator EuS. The shift of E_F from ~ 550 mV to ~34mV in superconducting SS is an important step towards realizing MBS in this robust system.

One Sentence Summary: Surface state superconductivity near the Kramer's degeneracy point of Rashba band in ultra-thin gold with strong spin-orbit coupling.

Main text:

The Shockley surface state (SS) of Au(111) is well-known to feature strong Rashba spin-orbit coupling (SOC) and recently has been predicted to have topological nature.[2,3] Such strong SOC, reaching 110 meV and orders of magnitude stronger than those in semiconductors, has been theoretically shown to produce robust MBS once the SS attains SC.[1] Several experiments have shown the potential signatures of MBS.[4-15] Achieving SC in SS of Au, therefore, will further lay the foundation for obtaining more robust MBS, for example a pair of MBS existing at higher temperatures. Besides, because the large-scale design and fabrication of nanowire network at the wafer-scale is possible with Au(111) thin film, this approach is scalable. These unique advantages would readily allow the Au(111) platform to realize a variety of proposed schemes to manipulate the MBS.

The SS band has no direct overlap with the projection of the bulk gold band on the (111) surface and the standard mechanism of superconducting proximity effect does not apply. Our prior theoretical work has shown that a finite superconducting pair amplitude is generated in SS through elastic or inelastic scattering processes even though the SS are not directly in touch with a superconductor.[1] Although it is not clear how this new mechanism will work in practice, it is important to demonstrate the superconductivity in SS experimentally. A second problem is that the Fermi energy of the SS is very large, ~550 meV, and holds many transverse sub-bands for any realistic nanowire width. It will be important to reduce the Fermi energy. In this paper we demonstrate that by depositing EuS on the gold surface, a giant shift from ~550 meV to ~34 meV is achieved. Further, EuS has the added advantage that it is a ferromagnet insulator and can enhance the Zeeman energy by exchange interaction. By using EuS as a barrier in tunnel junction,

we see evidence of the magnetism by change of coherence peak height as a function of the magnetic field.

We have achieved surface state SC by using pristine (111) surface of ultra-thin (4 nm) wafer-scale Au film grown on vanadium, a *s*-wave superconductor.[16] The film thickness ~ 4 nm is chosen so that the Au(111) layer thickness is much greater than the SS penetration depth (~3.2 monolayer),[17] and thin enough to allow fully induced SC gap in its bulk,[18] in contrast to the previous report on Ag(111) where the SS penetration depth is comparable to the layer thickness.[17,19] Our island-free Au(111) layer on V (Fig. 1) further allows uniformly induced SC gap, which could otherwise be degraded by island boundaries,[19-21] providing a stable platform for fabricating scalable Au nanowire network in the future for detecting and braiding the MBS.[1,22]

The high quality Au(111) layer, confirmed by atomically resolved STM topography (Fig. 1c and 1d), possesses clear SS. The bottom of the SS band (E_{SS}) manifests as a peak in dI/dV vs V_{bias} spectrum at V_{bias} ~ -0.57 eV (Fig. 1c inset and Fig. 2b). Compared to bulk Au crystals,[23,12] our measured E_{SS} is close but lower. This could be a result of the STM tip electric field affecting the SS, or could indicate that the value of E_{SS} may be different in 4nm Au(111) grown on V. At V_{bias} = 0 eV, where E_F is located, the Fermi level therefore crosses both bulk states and SS. It has been shown that the SS of a noble metal can degrade when growing on another metal and having a thickness comparable to the SS decaying depth.[17] The sharp dI/dV peak (Fig. 1c inset) demonstrates that the SS is well defined.

We show that $E_{SS} - E_F$ sensitively depends on the dielectric environment above the Au(111) surface (Fig. 2), an effect which is crucial for electronically manipulating MBS in future experiments.[1,24] We modulate E_F by growing ultra-thin EuS, a ferromagnetic high-κ dielectric insulator (ϵ ~ 23.9 in bulk),[25] on top of Au(111)/V (Fig. 2a). Rectangular shaped EuS islands

with uniform monolayer (ML) height (~2.8 Å) grow well on Au(111). In order to estimate how a ML of EuS affects the surface state of the underneath Au, we measure spectroscopy on top of EuS island and bare Au surface sequentially (see Fig. 2b). On both bare and EuS covered sites, dI/dV shows a peak at E_{SS} (Fig. 2b) as expected. Compared to bare Au, E_{SS} on EuS island is shifted upwards by ~200 meV towards E_F. We point out that the Au(111) surface has the same E_F regardless of whether it is with or without the coverage of EuS, whereas the reduced $|E_{SS} - E_F|$ is a result of the increase of E_{SS} due to EuS coverage. Because the SS are quantum well states confined by the *s-p* bulk band gap of Au and the surface image potential, the large dielectric constant of EuS modifies the image potential and reduces the quantum well width to deplete the surface electrons.[26] Unlike other reported approaches of tuning the SS band of Au(111), for example using monolayer MgO,[27] the magnetic EuS also generates a substantial interface Zeeman field (ZF), a prerequisite for creating MBS in Au(111).[1,28-31]

Next, we bring E_F further closer to the Kramers degeneracy point of SS by increasing EuS thickness. With thicker EuS layer scanning tunneling spectroscopy (STS) becomes impractical, so we fabricated planar thin film sandwich tunnel junctions (TJs) and perform dI/dV tunneling spectroscopy through the 2.4 nm thick EuS layer (Fig. 2c). In TJs, we observe that E_F approaches E_{SS} further with $|E_{SS} - E_F|$ ~ 34 meV (Fig. 2c), which is in the vicinity of the Kramers degeneracy point.[32] A sizable Zeeman field, such as that provided by the EuS layer,[28-30,33,34] is predicted to cause topological SC and MBS.[1] The depletion of the SS also serves to reduce the number of the SS sub-bands, leading to a much more favorable condition for the creation of MBS's. [1]

The induced bulk SC gap in the 4 nm Au(111) is expected to be governed by conventional proximity effect. According to McMillian's model,[18] when a normal metal is in contact with a superconductor, the normal metal obtains a proximity induced self-energy of:

$$\Delta_N = \frac{(\Gamma_S \Delta_N^{ph} + \Gamma_N \Delta_S^{ph})}{(\Gamma_S + \Gamma_N)} \quad (1)$$

where Δ_N^{ph} and Δ_S^{ph} denote the self-energies of the normal metal and the superconductor due to phonons ($\Delta_N^{ph} \sim 0$ for Au).[18] The energy scales Γ_N and Γ_S are defined as $\Gamma_N = \frac{\hbar}{\tau_N}$ and $\Gamma_S = \frac{\hbar}{\tau_S}$, where relaxation times τ_N and τ_S represent the time a quasiparticle spent in the Au(111) layer and the V layer respectively.[18] For films with a thickness d less than the mean-free-path l, we have $\tau \sim \frac{d}{v_F}$. Taking the literature values $v_F \sim 8\times10^5$ m/s in Au and $v_F \sim 1.8\times10^5$ m/s in V,[32,35] we find $\Gamma_N \gg \Gamma_S$ for 4nm Au(111) grown on 20nm V. Therefore, we expect $\Delta_N \approx \Delta_S^{ph}$ (Eq. 1) indicating that the bulk states of Au(111) inherit the full SC gap from V. Such conventional proximity effect is revealed by our TJs with EuS barrier, in which a SC gap shows up when T is below the T_C of Au(111)/V (Fig. 3a).[16]

As the temperature of the sample being lowered below 2.5 K, the dI/dV coherence peaks split (Fig. 3a). We attribute such splitting feature to indicate the emergence of a new SC gap in Au(111), and that it does not correspond to the lifted spin degeneracy in Au(111) under the magnetic exchange field (MEF) of EuS as previously seen in Al.[33] In materials with strong SOC, such as Au(111), spin is not a good quantum number and thus the spin splitting of the quasiparticle density-of-states (DOS) is suppressed in the presence of strong MEF, as has been demonstrated in Al TJs with Pt scatters.[36-42]

To confirm that the spin splitting is suppressed, the Al_2O_3/Al interface in a standard Al/Al_2O_3/Al/EuS junction is decorated with a sub-monolayer of Au (Fig. 3b and SI). The typical dI/dV spectra (Fig. 3b) show collapsed spin-split coherence peaks in the presence of only 0.6 Å Au at the interface. Using Maki-Fulde model,[43-47] we show that the spin-orbit scattering parameter b $(= \hbar/3\Delta\tau_{so})$, where τ_{so} is the spin-orbit scattering time and Δ is the superconductor gap, systematically increases when the Au thickness increases (SI) and the split coherence peaks in 4nm Au (Fig. 3a) could not be caused by MEF.[37-41] Hence the development of the second peak in Fig. 3a is attributed to the emergence of an additional SC gap that is opened up in Au(111) at temperatures below ~ 3K, lower than the bulk T_C ~ 4.0 K of Au(111)/V.

To better resolve the emergent SC gap, the sample is cooled down to T = 1.0 K (Fig. 3c) and we observe four dI/dV peaks labeled as B_+, S_+, B_- and S_- representing the sum (+) and difference (-) tunneling processes in a S-I-S TJ. The dI/dV spectrum can be modeled by considering two SC gaps in the Au(111) layer: bulk gap (B) and surface gap (S) (Fig. 3d). The total quasiparticle DOS in Au(111) can be written as the sum of two BCS terms, i.e. one from bulk (B) and one from surface (S), as:

$$\left(\frac{1+r}{2}\right) \cdot Re\left(\frac{E-i\Gamma_B}{\sqrt{(E-i\Gamma_B)^2-\Delta_B^2}}\right) + \left(\frac{1-r}{2}\right) \cdot Re\left(\frac{E-i\Gamma_S}{\sqrt{(E-i\Gamma_S)^2-\Delta_S^2}}\right) \quad (2)$$

with r adjusting the ratio of the two, and Γ the lifetime of the quasiparticles. The model (Eq. 2) reproduces the position and the relative magnitudes of the dI/dV peaks (Fig. 3c). We thereby extract the SC gaps as: Δ_B = 0.63 ± 0.04 meV, Δ_{Al} = 0.22 ± 0.04 meV, and Δ_S = 0.38 ± 0.02 meV. Both the bulk gap (Δ_B) and the Al gap (Δ_{Al}), as expected, nicely agree with the BCS relation $2\Delta = 3.5k_BT_C$ (Au/V T_C ~ 4.0 K and Al T_C ~ 1.7 K). The bulk gap Δ_B seen in Fig 3a originates from the induced bulk SC due to the conventional proximity effect as describe by Eq. 1. On the

other hand, Δ_S, with a smaller size, has to come from a different energy band in Au (111). Since E_F crosses both bulk and surface bands (Fig. 2c and 2d), Δ_S is a result of the induced SC in the SS of Au(111). As discussed previously, the SS has a penetration depth of only ~ 3.2 monolayers in Au(111),[48] and is thus well separated from V by the 4nm thick Au(111) layer. Conventional proximity effect (Eq. 1) cannot account for this. Furthermore, the SS band lies within a large gap of the bulk bands when projected to the (111) surface which is responsible for the well-defined nature of the SS. This also means that direct single electron hopping is not possible between the surface and the bulk. Thus, the gap Δ_S must be induced indirectly – concurring with our previous theoretical predictions.[17] The idea is that while a single electron in the SS has no overlap with the bulk electronic state, a pair of SS electrons can couple to a Cooper pair in the bulk via elastic scattering from impurities or inelastic scattering due to phonons or Coulomb interactions. We point out that the peaks S_+, B_- and S_- do not result from the sub-gap bound states caused by Andreev reflections as explained below. Such bound states would satisfy the De Gennes - St. James equation as: $\frac{\varepsilon_n L}{\hbar v_F} = n\pi + \cos^{-1}\left(\frac{\varepsilon_n}{\Delta}\right)$ with ε_n the energy of the bound states, L the trajectory length of the coherent Andreev pairs, and Δ the main SC gap ($\Delta = \Delta_B$ in our case).[1] However, if we assume S_-, the peak positions of other sub-gap peaks (S_+ and B_-) cannot be reproduced by the De Gennes - St. James equation. Moreover, as shown in Fig. 3c, the tunneling conductance at B_+ is at least four times larger than those of the other peaks. This excludes also the possibility that they are contributed by the spin-split coherence peaks of Al under the MEF of EuS.[49] Therefore, the emergence of Δ_S is clearly attributable to the induced SC in the SS of Au(111).

The SC in SS further demonstrates contrasting properties under an external magnetic field suggesting its 2D nature. We apply a magnetic field $\boldsymbol{B}_{\parallel}$ of 270 Oe parallel to the film plane

of the junction (Fig. 4a), large enough to align EuS magnetization.[36] The peak heights at B_+ and B_- drop noticeably under $\boldsymbol{B}_{\parallel}$ (Fig. 4b) as a result of the orbital depairing effects. Because B_+ and B_- correspond to the quasiparticle tunneling between the bulk states of Au(111) and Al, the enhanced depairing reflects the weakening of bulk SC.[31] However, the S_+ and S_- peaks are noticeably increased (Fig. 4b) suggesting an improved quasiparticle lifetime, and which cannot be attributed to the tunneling of bulk states with $\boldsymbol{B}_{\parallel}$ present. However, it is known that the depairing effect can be largely suppressed in superconductors approaching the 2D limit, where the thicknesses of the superconductor is smaller than the penetration depth of a parallel magnetic field.[36] Therefore, S_+ and S_- could involve the tunneling of 2D-like quasiparticles such as those from the SS of Au(111).[36] Moreover, the field$\boldsymbol{B}_{\parallel}$ aligns the magnetization of EuS. Before the application of $\boldsymbol{B}_{\parallel}$, the non-aligned spins at the EuS/Au(111) interface and domain walls present in EuS can introduce spin-flip scattering, which reduces the quasiparticle lifetime of SS. The enhanced S_+ and S_- peaks suggest the aligned interface spins and the magnetized EuS, further supporting the 2D nature of SS.

Interestingly, we observe an additional dI/dV peak at zero voltage (Fig. 3c), which doesn't decay when $\boldsymbol{B}_{\parallel}$ is applied, while it disappears when $\boldsymbol{B}_{\perp}$ is applied. Our model in Eq. (2) cannot account for this dI/dV peak. We suggest that this dI/dV peak could be due to Andreev reflections, which cause the tunneling of Cooper pairs between the top electrode Al and the bottom electrode Au. Nevertheless, the physical origin of this dI/dV peak requires further studies. Our demonstrated SC in the Au(111) SS sets the stage for the observation of MBS in tunable and scalable EuS/Au(111)/V layered system.

Methods:

We use similar growth method as reported before.[17] Scanning tunneling spectroscopy (STS) and scanning electron microscopy (SEM) are used to confirm the high quality Au(111) surface. The STM and STS experiments are performed in a custom assembled STM with RHK PanScan head integrated in a Janis 300mK He^3 cryostat with vector magnet. Atomically resolved STM images of Au(111) surface are obtained after the growth by careful pumping of the sample space in the STM load-lock with a turbo molecular pump. The spectroscopy of differential conductance dI/dV versus bias voltage is performed at T = 5K under open feedback loop condition with a voltage modulation V_{rms} ~ 7-10 mV and AC frequency f = 1.57 KHz.

Figures and Captions:

Fig. 1

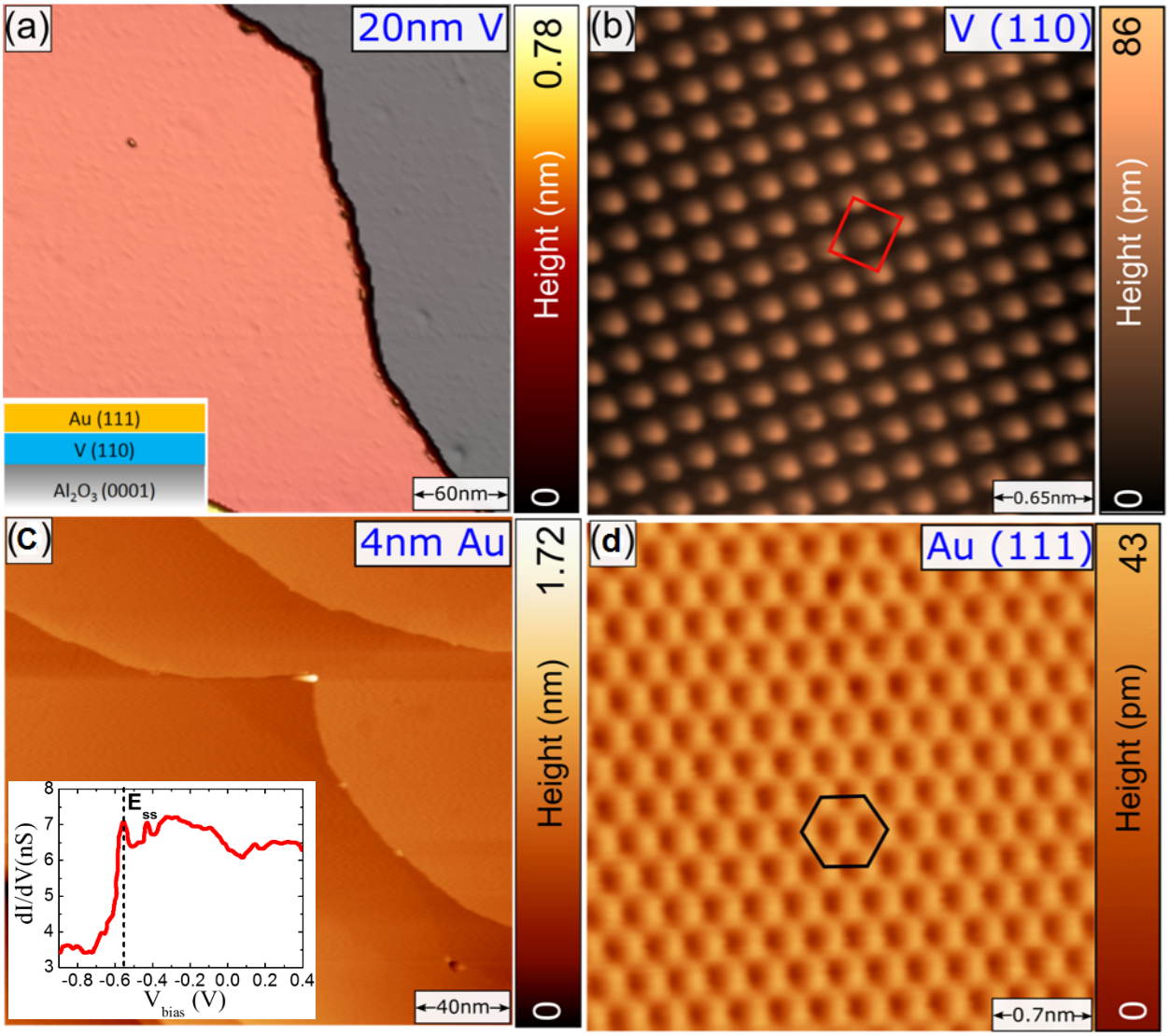

Fig. 2

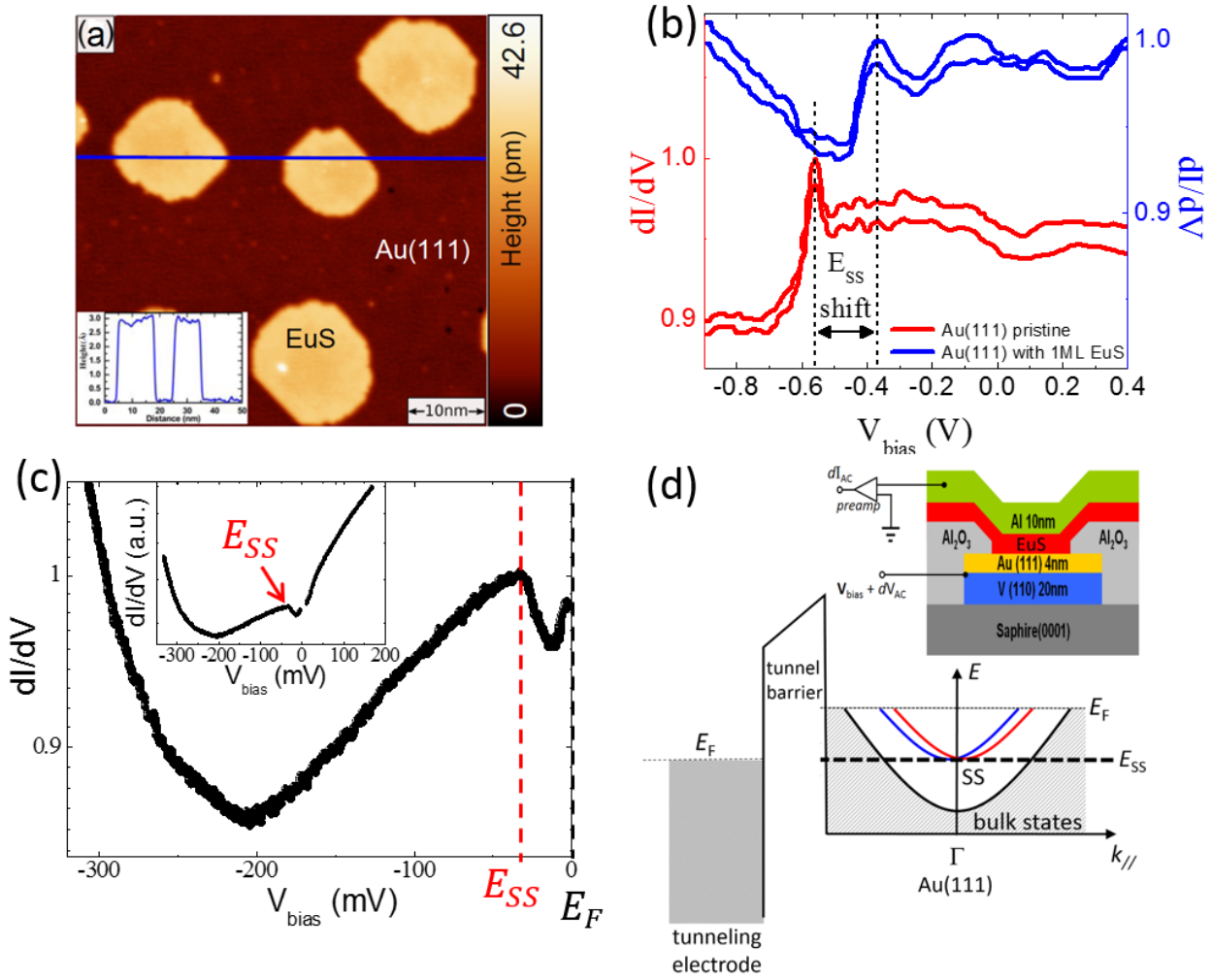
(a)
Au(111)
EuS
10nm
Height (pm)
42.6
0
(b)
dI/dV
ΔP/IP
1.0
0.9
E_SS
shift
Au(111) pristine
Au(111) with 1ML EuS
-0.8 -0.6 -0.4 -0.2 0.0 0.2 0.4
V_bias (V)
(c)
dI/dV
dI/dV (a.u.)
E_SS
V_bias (mV)
-300 -200 -100 0
E_F
(d)
dI_AC
preamp
V_bias + dV_AC
Al 10nm
Al2O3
EuS
Au (111) 4nm
V (110) 20nm
Saphire(0001)
tunnel barrier
E_F
E_SS
SS
bulk states
Γ
k//
Au(111)
tunneling electrode

Fig. 3

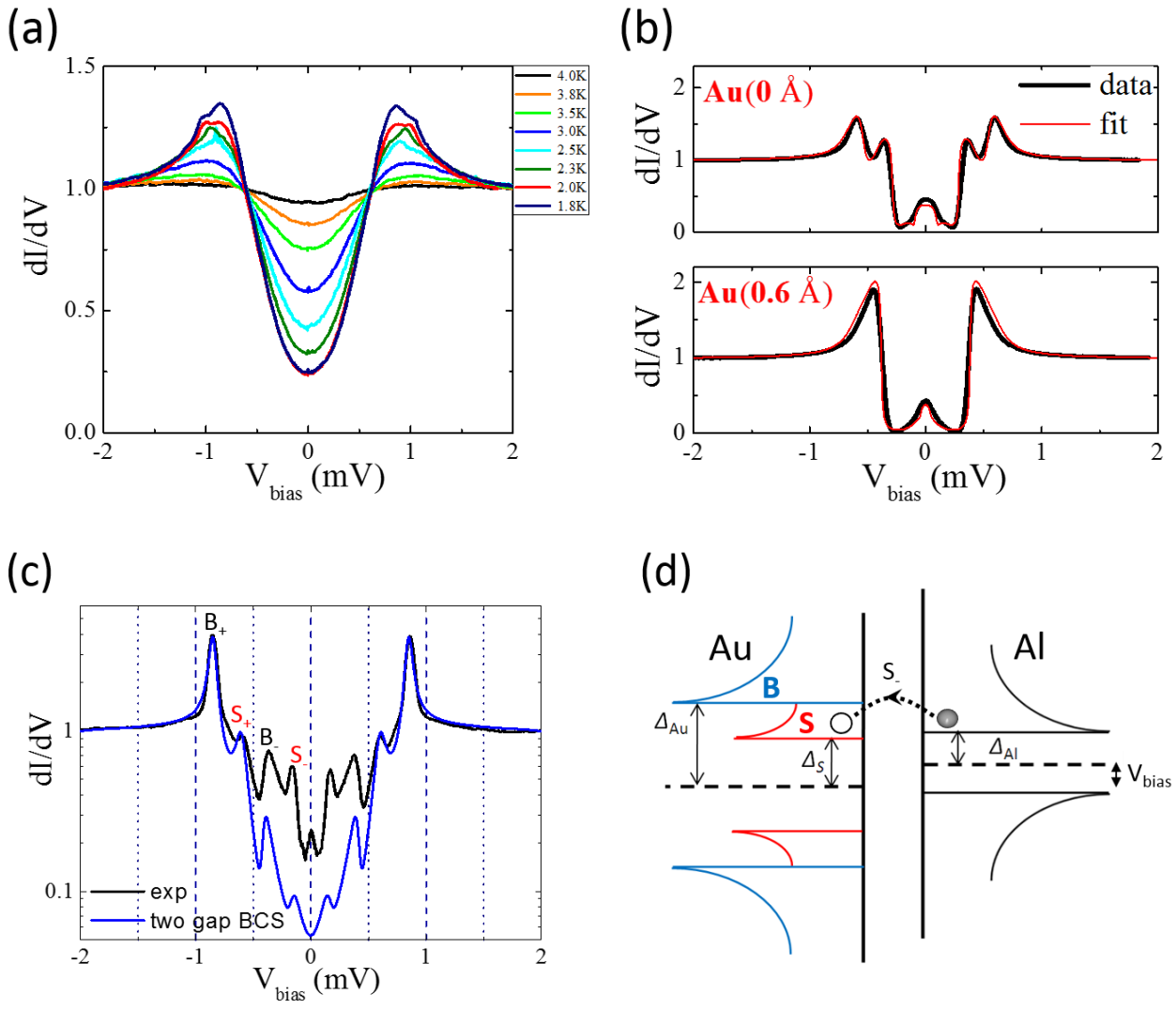
(a)
dI/dV
V bias (mV)
4.0K
3.8K
3.5K
3.0K
2.5K
2.3K
2.0K
1.8K
(b)
Au(0 Å)
Au(0.6 Å)
data
fit
dI/dV
V bias (mV)
(c)
B+
S+
B-
S-
exp
two gap BCS
dI/dV
V bias (mV)
(d)
Au
Al
B
S
S-
Δ Au
Δ S
Δ Al
V bias

Fig. 4

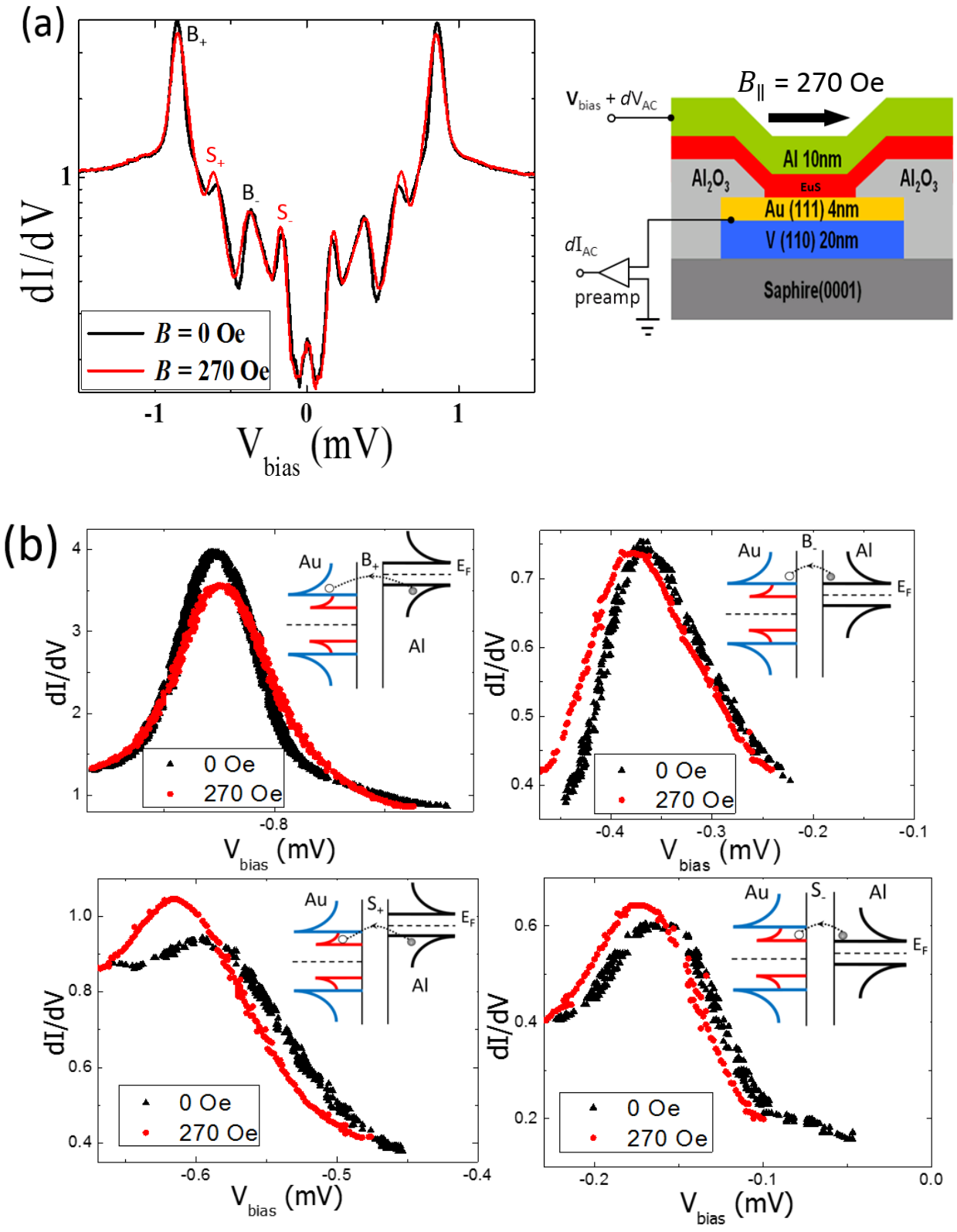
(a)
B+
S+
B-
S-
dI/dV
1
-1
0
1
V bias (mV)
B = 0 Oe
B = 270 Oe
V bias + dV AC
B|| = 270 Oe
Al 10nm
Al2O3
EuS
Al2O3
Au (111) 4nm
V (110) 20nm
dI AC
preamp
Saphire(0001)
(b)
Au
B+
E F
Al
0 Oe
270 Oe
V bias (mV)
Au
B-
Al
E F
S+
S-

Fig. 1: (a) Large scale constant current STM topography image of 20nm thick V film grown on sapphire substrate. (Inset): schematic layout of the heterostructure. **(b)** High resolution STM image confirming V(110) surface.[16] **(c)** The large scale atomic terraces of 4nm Au grown on V. (Inset): dI/dV tunneling spectrum showing the edge of the surface energy band. **(d)** Atomic resolved STM image showing the hexagonal atomic lattice of Au(111).

Fig. 2: (a) STM topography image of sub-ML EuS grown on Au(111)/V surface. A continuous EuS layer is obtained when the thickness is above 3ML (~1nm), which causes difficulties for the STM scanning due to insulating EuS. The line scan profile (inset) shows the height of the EuS island is ~ 3Å. **(b)** STS spectrum obtained on top of pristine Au(111) (red) and on Au(111) with 1ML EuS island (blue) respectively. The bottom of the SS band shifts towards E_F by ~ 0.2 eV. The tunneling spectra are normalized to the dI/dV peaks respectively. In each case, two dI/dV scans (manually shifted on the vertical axis) are shown to demonstrate the reproducibility. **(c)** With 2.4 nm EuS grown on Au(111), E_F is found to be only ~ 34 meV above E_{SS}. Because 2.4 nm EuS is insulating, the dI/dV spectra are measured in planar tunnel junction (TJ) devices. The tunneling spectrum is normalized to the dI/dV peak that corresponds to E_{SS}. The inset shows the dI/dV spectrum in the full bias voltage range. The clear asymmetry (inset), showing the dI/dV peak only at the negative bias voltage side, is consistent to our tunneling experiment setup and the band structure of Au(111), which are shown in (d).

Fig. 3: (a) $\boldsymbol{dI/dV}$ of the TJ shown in Fig. 2c inset (EuS thickness: 2.4 nm). Because $\boldsymbol{dI/dV}$ depends on the DOS of the two layers (Au and Al) in the vicinity of the insulating barrier EuS, the $\boldsymbol{dI/dV}$ gap reflects the induced SC in bulk Au(111). The doublet on the coherence peak is a

signature of the SS gap. **(b)** A control sample showing that the doublet is not due to the MEF of EuS. The control TJs have one Al tunneling electrode coupled to EuS with decorated Au to tune the interface SOC (noted as $Al/Al_2O_3/Au/Al/EuS$). **(c)** $\boldsymbol{dI/dV}$ of the same device as in **(a)** measured at T = 1.0 K (black curve). The multiple conductance peaks are well modeled (blue curve) by the S-I-S tunneling of the two band SC in Au (111) (Fig. 3d). **(d)** Schematics of the S-I-S tunneling model with Au having two induced SC gaps.

Fig. 4: (a) Tunneling conductance of planar TJ (schematic on the right) in the presence of a parallel magnetic field. Half of the tunneling peaks demonstrate contrasting responses to the magnetic field. **(b)** The zoomed-in data of each tunneling peak. For tunneling involving the bulk quasiparticles of Au, the conductance peak (red curves) is reduced by the applied magnetic field. For tunneling involving the SS quasiparticles of Au, the conductance peak (red curves) is enhanced by the applied magnetic field, which indicates the 2D nature of the quasiparticles in SS.

Acknowledgments:

P.W., S.M., P.L. and J.S.M. would like to acknowledge the support from John Templeton Foundation Grant Nos. 39944 and 60148. P.W., S.M. and J.S.M. would like to acknowledge Office of Naval Research Grant N00014-13-1-0301 and N00014-16-1-2657 and National Science Foundation Grant DMR-1207469 and DMR-1700137.

References:

1 Potter, A. C. & Lee, P. A. Topological superconductivity and Majorana fermions in metallic surface states. *Phys Rev B* **85**, 094516, (2012).

2 LaShell, S., McDougall, B. A. & Jensen, E. Spin Splitting of an Au(111) Surface State Band Observed with Angle Resolved Photoelectron Spectroscopy. *Phys Rev Lett* **77**, 3419, (1996).

3 Yan, B. *et al.* Topological states on the gold surface. *Nat Commun* **6**, (2015).

4 Mourik, V., Zuo, K., Frolov, S. M., Plissard, S. R., Bakkers, E. P. A. M. & Kouwenhoven, L. P. Signatures of Majorana Fermions in Hybrid Superconductor-Semiconductor Nanowire Devices. *Science* **336**, 1003-1007, (2012).

5 Rokhinson, L. P., Liu, X. & Furdyna, J. K. The fractional a.c. Josephson effect in a semiconductor-superconductor nanowire as a signature of Majorana particles. *Nat Phys* **8**, 795-799, (2012).

6 Das, A., Ronen, Y., Most, Y., Oreg, Y., Heiblum, M. & Shtrikman, H. Zero-bias peaks and splitting in an Al-InAs nanowire topological superconductor as a signature of Majorana fermions. *Nat Phys* **8**, 887-895, (2012).

7 Deng, M. T., Yu, C. L., Huang, G. Y., Larsson, M., Caroff, P. & Xu, H. Q. Anomalous Zero-Bias Conductance Peak in a Nb–InSb Nanowire–Nb Hybrid Device. *Nano Lett* **12**, 6414-6419, (2012).

8 Finck, A. D. K., Van Harlingen, D. J., Mohseni, P. K., Jung, K. & Li, X. Anomalous Modulation of a Zero-Bias Peak in a Hybrid Nanowire-Superconductor Device. *Phys Rev Lett* **110**, 126406, (2013).

9 Albrecht, S. M., Higginbotham, A. P., Madsen, M., Kuemmeth, F., Jespersen, T. S., Nygård, J., Krogstrup, P. & Marcus, C. M. Exponential protection of zero modes in Majorana islands. *Nature* **531**, 206-209, (2016).

10 Nadj-Perge, S., Drozdov, I. K., Li, J., Chen, H., Jeon, S., Seo, J., MacDonald, A. H., Bernevig, B. A. & Yazdani, A. Observation of Majorana fermions in ferromagnetic atomic chains on a superconductor. *Science* **346**, 602-607, (2014).

11 Deng, M. T., Vaitiekėnas, S., Hansen, E. B., Danon, J., Leijnse, M., Flensberg, K., Nygård, J., Krogstrup, P. & Marcus, C. M. Majorana bound state in a coupled quantum-dot hybrid-nanowire system. *Science* **354**, 1557, (2016).

12 Sun, H.-H. *et al.* Majorana Zero Mode Detected with Spin Selective Andreev Reflection in the Vortex of a Topological Superconductor. *Phys Rev Lett* **116**, 257003, (2016).

13 He, Q. L. *et al.* Chiral Majorana fermion modes in a quantum anomalous Hall insulator–superconductor structure. *Science* **357**, 294, (2017).

14 Zhang, H. *et al.* Quantized Majorana conductance. *Nature* **556**, 74, (2018).

15 Lutchyn, R. M., Bakkers, E. P. A. M., Kouwenhoven, L. P., Krogstrup, P., Marcus, C. M. & Oreg, Y. Majorana zero modes in superconductor–semiconductor heterostructures. *Nature Reviews Materials* **3**, 52-68, (2018).

16 Wei, P., Katmis, F., Chang, C.-Z. & Moodera, J. S. Induced Superconductivity and Engineered Josephson Tunneling Devices in Epitaxial (111)-Oriented Gold/Vanadium Heterostructures. *Nano Lett* **16**, 2714-2719, (2016).

17 Hsieh, T. C. & Chiang, T. C. Spatial dependence and binding energy shift of surface states for epitaxial overlayers of Au on Ag(111) and Ag on Au(111). *Surf Sci* **166**, 554-560, (1986).

18 McMillan, W. L. Tunneling Model of the Superconducting Proximity Effect. *Phys Rev* **175**, 537-542, (1968).

19 Tomanic, T., Schackert, M., Wulfhekel, W., Sürgers, C. & Löhneysen, H. v. Two-band superconductivity of bulk and surface states in Ag thin films on Nb. *Phys Rev B* **94**, 220503, (2016).

20 Gupta, A. K., Crétinon, L., Moussy, N., Pannetier, B. & Courtois, H. Anomalous density of states in a metallic film in proximity with a superconductor. *Phys Rev B* **69**, 104514, (2004).

21 Wolz, M., Debuschewitz, C., Belzig, W. & Scheer, E. Evidence for attractive pair interaction in diffusive gold films deduced from studies of the superconducting proximity effect with aluminum. *Phys Rev B* **84**, 104516, (2011).

22 Hyart, T., van Heck, B., Fulga, I. C., Burrello, M., Akhmerov, A. R. & Beenakker, C. W. J. Flux-controlled quantum computation with Majorana fermions. *Phys Rev B* **88**, 035121, (2013).

23 Kliewer, J., Berndt, R., Chulkov, E. V., Silkin, V. M., Echenique, P. M. & Crampin, S. Dimensionality Effects in the Lifetime of Surface States. *Science* **288**, 1399-1402, (2000).

24 Aasen, D. *et al.* Milestones Toward Majorana-Based Quantum Computing. *Physical Review X* **6**, 031016, (2016).

25 Mauger, A. & Godart, C. The magnetic, optical, and transport properties of representatives of a class of magnetic semiconductors: The europium chalcogenides. *Physics Reports* **141**, 51-176, (1986).

26 Smith, N. V. Phase analysis of image states and surface states associated with nearly-free-electron band gaps. *Phys Rev B* **32**, 3549-3555, (1985).

27 Pan, Y., Benedetti, S., Nilius, N. & Freund, H.-J. Change of the surface electronic structure of Au(111) by a monolayer MgO(001) film. *Phys Rev B* **84**, 075456, (2011).

28 Wei, P. *et al.* Strong interfacial exchange field in the graphene/EuS heterostructure. *Nat Mater* **15**, 711, (2016).

29 Katmis, F. *et al.* A high-temperature ferromagnetic topological insulating phase by proximity coupling. *Nature* **533**, 513, (2016).

30 Wei, P., Katmis, F., Assaf, B. A., Steinberg, H., Jarillo-Herrero, P., Heiman, D. & Moodera, J. S. Exchange-Coupling-Induced Symmetry Breaking in Topological Insulators. *Phys Rev Lett* **110**, 186807, (2013).

31 Moodera, J. S., Santos, T. S. & Nagahama, T. The phenomena of spin-filter tunnelling. *J Phys-Condens Mat* **19**, 165202, (2007).

32 Nicolay, G., Reinert, F., Hufner, S. & Blaha, P. Spin-orbit splitting of the L-gap surface state on Au(111) and Ag(111). *Phys Rev B* **65**, 033407, (2001).

33 Hao, X., Moodera, J. S. & Meservey, R. Thin-film superconductor in an exchange field. *Phys Rev Lett* **67**, 1342-1345, (1991).

34 Li, B., Roschewsky, N., Assaf, B. A., Eich, M., Epstein-Martin, M., Heiman, D., Münzenberg, M. & Moodera, J. S. Superconducting Spin Switch with Infinite Magnetoresistance Induced by an Internal Exchange Field. *Phys Rev Lett* **110**, 097001, (2013).

35 Radebaugh, R. & Keesom, P. H. Low-Temperature Thermodynamic Properties of Vanadium. II. Mixed State. *Phys Rev* **149**, 217-231, (1966).

36 Meservey, R. & Tedrow, P. M. Spin-polarized electron tunneling. *Physics Reports* **238**, 173-243, (1994).

37 Bruno, R. C. & Schwartz, B. B. Magnetic Field Splitting of the Density of States of Thin Superconductors. *Phys Rev B* **8**, 3161-3178, (1973).

38 Meservey, R., Tedrow, P. M. & Bruno, R. C. Tunneling measurements on spin-paired superconductors with spin-orbit scattering. *Phys Rev B* **11**, 4224-4235, (1975).

39 Worledge, D. C. & Geballe, T. H. Maki analysis of spin-polarized tunneling in an oxide ferromagnet. *Phys Rev B* **62**, 447-451, (2000).

40 Tedrow, P. M. & Meservey, R. Critical magnetic field of very thin superconducting aluminum films. *Phys Rev B* **25**, 171-178, (1982).

41 Tedrow, P. M. & Meservey, R. Experimental Test of the Theory of High-Field Superconductivity. *Phys Rev Lett* **43**, 384-387, (1979).

42 Xi, X., Wang, Z., Zhao, W., Park, J.-H., Law, K. T., Berger, H., Forro, L., Shan, J. & Mak, K. F. Ising pairing in superconducting NbSe2 atomic layers. *Nat Phys* **12**, 139-143, (2016).

43 Maki, K. Pauli Paramagnetism and Superconducting State. II. *Prog Theor Phys* **32**, 29-36, (1964).

44 Fulde, P. & Maki, K. Theory of Superconductors Containing Magnetic Impurities. *Phys Rev* **141**, 275-280, (1966).

45 Meservey, R., Tedrow, P. M. & Fulde, P. Magnetic Field Splitting of the Quasiparticle States in Superconducting Aluminum Films. *Phys Rev Lett* **25**, 1270-1272, (1970).

46 Fulde, P. High field superconductivity in thin films. *Adv Phys* **22**, 667-719, (1973).

47 Alexander, J. A. X., Orlando, T. P., Rainer, D. & Tedrow, P. M. Theory of Fermi-liquid effects in high-field tunneling. *Phys Rev B* **31**, 5811-5825, (1985).

48 Dynes, R. C., Narayanamurti, V. & Garno, J. P. Direct Measurement of Quasiparticle-Lifetime Broadening in a Strong-Coupled Superconductor. *Phys Rev Lett* **41**, 1509-1512, (1978).

49 De Gennes, P. G. & Saint-James, D. Elementary excitations in the vicinity of a normal metal-superconducting metal contact. *Phys Lett* **4**, 151-152, (1963).